

# Numerical model of multi-ion transport in concrete during electrochemical lithium migration

Lourdes M. S. Souza <sup>1,2</sup>, Rob B. Polder <sup>1,3</sup>, Oguzhan Çopuroğlu <sup>1</sup>

<sup>1</sup> Faculty of Civil Engineering and Geosciences, Delft University of Technology, the Netherlands

<sup>2</sup> Tecgraf Institute, Pontifical Catholic University of Rio de Janeiro, Brazil

<sup>3</sup> RPCP, Gouda, the Netherlands

Electrochemical lithium migration has been investigated as a possible treatment for concrete structures affected by alkali-silica reaction (ASR) by several authors. However, there is still no consensus on its effectiveness. Understanding the mechanisms behind lithium migration and its numerical modelling are essential in order to explore feasibility of lithium treatment in ASR affected concrete.

In this paper, a mathematical model for multi-ion transport in concrete (or mortar) is presented. A multi-ion model was considered as the presence of other ions in the pore solution may influence lithium transport. The model was numerically implemented for two-chamber migration experiments with mortar specimens. The experiments were conducted during a week under 40 V and LiOH solutions were used as anolyte. The model predicted well the final lithium content in the specimens. It also indicated that the removal of all sodium and potassium ions was necessary before lithium reached the catholyte chamber.

*Keywords: Alkali-silica reaction, migration, lithium-based treatment, numerical modelling*

## 1 Introduction

Electrochemical lithium migration has been investigated by numerous authors as a possible treatment against alkali-silica reaction (ASR) in existing concrete structures (e.g. [1-7]). Lithium ions are acknowledged to prevent ASR expansion in new concrete by altering the reaction mechanism, forming a less expansive product or hindering its formation [8-12]. In existing structures, lithium needs to be transported into the hardened concrete, and migration (i.e. ionic transport under an electric field) has been considered the

method that leads to higher concentration and extended depth of penetration [1, 2].

However, current studies present various different procedures and there is no consensus on whether the treatment effectively suppresses ASR expansion.

Numerical modelling can be a useful tool to predict ionic transport rates in cement-based materials. In fact, in the past years, a variety of models has been proposed, mostly to describe the transport (ingress or removal) of chloride in concrete e.g. [13–18]. Even though most models use the mass balance equation (Nernst-Planck) to describe the movement of species in solution, different approaches are employed.

Many studies only consider the ion of interest - the effect of the interaction between species is neglected and one mass balance equation is used (e.g. [13–15]). On the other hand, simulations that take into consideration different ions in the pore solution (e.g. sodium, potassium, hydroxyl) become more complex, as they demand a separate mass balance equation for each species. Moreover, they also consider electroneutrality of the electrolyte, in an additional equation (e.g. [16–18]). A further step is taken when those species are no longer considered inert: they either leave or enter the pore solution by chemical reactions or physical adsorption. In models describing chloride movement, binding may be included (e.g. [14,16]).

In this paper, a mathematical model for multi-ion transport in cementitious materials was presented. This type of model was considered because the presence of other ions in the pore solution might influence lithium transport. The model was numerically implemented for two-chamber migration experiments with mortar specimens presented in [19]. Finally, the model results are compared with experimental findings.

## 2 Mathematical model

In order to describe the mass transfer process in a solution, it is necessary to describe the movement of ions, mass balances, current flow and electroneutrality [20]. Considering the flux of particles due to advection, diffusion and migration, the conservation of mass is described by the Nernst-Planck equation, shown in Eq.(1). In the case of charged particles, the variation of concentrations must also follow the electroneutrality principle, shown in Eq.(2). Finally, the current density  $i_c$  (in A/m<sup>2</sup>) in the electrolyte is due to the movement of the charged particles and it is expressed by Eq.(3) [20]:

$$\frac{\partial c_i}{\partial t} = -\nabla(c_i u - D_i \nabla c_i - u_{m,i} c_i \nabla \phi) + R_i \quad (1)$$

$$\sum_{i=1}^n z_i c_i = 0 \quad (2)$$

$$i_c = F \sum_{i=1}^n z_i (c_i u - D_i \nabla c_i - u_{m,i} c_i \nabla \phi) \quad (3)$$

where  $c_i$  is the concentration of the species  $i$  (in mol/m<sup>3</sup>),  $u$  is the velocity of the fluid (in m/s),  $D_i$  is the diffusion coefficient of species  $i$  (in m<sup>2</sup>/s),  $u_{m,i}$  is the ionic mobility (in m<sup>2</sup>/s.V),  $\phi$  is the electric potential (in V),  $R_i$  is reaction term (in mol/m<sup>3</sup>.s),  $z_i$  is the valence of ion  $i$  and  $F$  is the Faraday constant (96485 C/mol).

The ionic mobility of an ion is related to its size, including its adherent water molecules. It is defined as the velocity of the ion in an electric field of unit strength. Table 1 presents the ionic mobility of some ions.

The diffusion coefficient of an ion is related to the ionic mobility by the Nernst-Einstein equation [20]:

$$D_i = RT \frac{u_{m,i}}{z_i F} \quad (4)$$

where  $R$  is the universal gas constant (8.314 J/K.mol),  $T$  is the absolute temperature, in K;  $z_i$  is the valence of ion  $i$  and  $F$  is the Faraday constant (96485 C/mol).

Table 1: Ionic mobilities in water at 25 °C [21, 22]

| Cation (+)      | Ionic Mobility<br>(m <sup>2</sup> /s.V) | Anion (-)                    | Ionic Mobility<br>(m <sup>2</sup> /s.V) |
|-----------------|---|------------------------------|---|
| H <sup>+</sup>  | 36.30 x 10 <sup>-8</sup>                | OH <sup>-</sup>              | 20.52 x 10 <sup>-8</sup>                |
| K <sup>+</sup>  | 7.62 x 10 <sup>-8</sup>                 | SO <sub>4</sub> <sup>=</sup> | 8.27 x 10 <sup>-8</sup>                 |
| Li <sup>+</sup> | 4.01 x 10 <sup>-8</sup>                 | Cl <sup>-</sup>              | 7.91 x 10 <sup>-8</sup>                 |
| Na <sup>+</sup> | 5.19 x 10 <sup>-8</sup>                 | NO <sub>3</sub> <sup>-</sup> | 7.40 x 10 <sup>-8</sup>                 |

The principles previously described are also valid for porous materials, such as concrete or mortar. However, in this case, transport takes place in the water-filled pores. Therefore, species are no longer able to advance along the shortest path, like in bulk solutions. In fact,

transport in this type of materials is two to three orders of magnitudes lower than compared to bulk solution [22].

It is generally accepted that the transport in a porous medium is affected by parameters such as porosity, degree of saturation, tortuosity and constrictivity [23]. Tortuosity can be explained as the ratio between the actual length of the pore and the linear distance between the ends of it. Constrictivity, on the other hand, deals with the hindering in flow due to variations in the cross-sectional area of the pore. The factor that takes into account these properties is the effective transport coefficient [23], described below:

$$K^* = \frac{p\theta}{\tau_c} \quad (5)$$

where  $p$  is the porosity;  $\theta$  is the saturation degree and  $\tau_c$  is the tortuosity-constrictivity factor. The tortuosity-constrictivity factor can be estimated as the ratio between the theoretical (calculated considering the capillary pores as cylindrical tubes) and measured conductivity values ( $\kappa_t$  and  $\kappa_{exp}$ , respectively, both in S/m). The conductivity of the bulk solution can be calculated by [20]:

$$\kappa = F \sum_{i=1}^n z_i u_{m,i} c_i \quad (6)$$

And, the theoretical conductivity of the specimen can be defined as:

$$\kappa_t = \theta p F \sum_{i=1}^n z_i u_{m,i} c_i \quad (7)$$

Therefore, tortuosity-constrictivity factor is obtained by:

$$\tau_c = \frac{\kappa_{exp}}{\kappa_t} \quad (8)$$

The advective term (in m/s) can be considered as a combination of transport due to gradients of degree of saturation and electroosmosis [23]. Thus, the ionic transport in a porous material can be described by the modified Nernst-Planck equation:

$$\frac{\partial(p\theta)c_i}{\partial t} = -\nabla(K^*c_iD_\theta\nabla\theta - K^*D_i\nabla c_i - K^*(u_{m,i} + K_{e.o.})c_i\nabla\phi) + (p\theta)R_i \quad (9)$$

where  $D_\theta$  is the water diffusivity coefficient, in  $\text{m}^2/\text{s}$  and  $K_{e.o.}$  is the electroosmotic permeability, in  $\text{m}^2\text{s}^{-1}\text{V}^{-1}$ .

### 3 Migration experiment

The migration experiments were performed in two-chamber set-ups similar to the one described by ASTM 1202 [24]. In this type of set-up, a cylindrical specimen is positioned between two acrylic chambers filled with electrolytes (270 ml), each with a stainless steel mesh working as an electrode, as represented in the scheme of Figure 1. As an electric potential was applied between the electrodes, cations moved towards the cathode (negative electrode) while anions were attracted towards the anode (positive electrode).

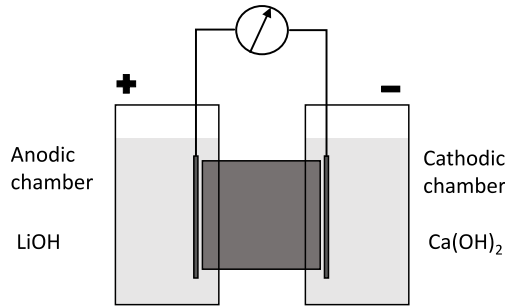


Figure 1: Schematic representation of the experimental set-up

The specimens were mortar cylinders (98 mm of diameter and 50 mm of height), with water to cement ratio of 0.50 and sand to cement mass proportion of 3:1. They were cured in a fog room ( $20.0 \pm 2.0$  °C and R.H. of  $96.0 \pm 2.0$  %) during 36 days. Portland cement type CEM I 42.5 N, CEN standard sand with  $D_{\max}$  of 2.0 mm (according to NEN-EN 196-1 [25]), and deionized water were used. The chemical composition of the cement is shown in Table 2.

Table 2: Cement composition, wt. % of cement

| CaO   | SiO <sub>2</sub> | Al <sub>2</sub> O <sub>3</sub> | Fe <sub>2</sub> O <sub>3</sub> | SO <sub>3</sub> | MgO  | P <sub>2</sub> O <sub>5</sub> | K <sub>2</sub> O | TiO <sub>2</sub> | Na <sub>2</sub> O | Other | L.O.I. <sup>1</sup> |
|-------|------------------|--------------------------------|--------------------------------|-----------------|------|-------------------------------|------------------|------------------|-------------------|-------|---------------------|
| 65.00 | 18.33            | 4.42                           | 3.38                           | 3.01            | 2.02 | 0.57                          | 0.46             | 0.37             | 0.28              | 0.53  | 1.60                |

<sup>1</sup> L.O.I.: loss on ignition

The experiments were carried out in a climate controlled laboratory, at  $20.0 \pm 2.0$  °C and R.H. of  $50.0 \pm 5.0$  %. Two LiOH solutions were used as anolyte: one with 4.9 M concentration (near saturation point) and another with 0.2 M. Saturated  $\text{Ca}(\text{OH})_2$  solution (0.02 M) was used as catholyte in all tests. Two specimens (replicates) per anolyte concentration were tested. However, due to experimental problems during testing with 0.2 M LiOH, the results of one specimen was considered. The specimens were tested under 40 V during a week. This voltage was chosen as it is the usual maximum voltage used in the field in treatments such as electrochemical chloride removal [22]. Passing current was continuously monitored and recorded by a data logger.

Samples from the electrolytes were collected during the experiment and were analysed by inductively coupled plasma optical emission spectroscopy (ICP-OES), in order to obtain the concentration of sodium, potassium, lithium and calcium (the last only in anolyte). Ionic content profiles were obtained after testing. The specimens were ground in a profile grinder in steps of 5.0 mm. The obtained powder was then dissolved in 3.0 M  $\text{HNO}_3$  and filtered to obtain a clear solution, which was analyzed by ICP-OES for lithium, sodium and potassium.

#### 4 Numerical implementation

The initial pore solution composition was estimated using values found in [16] and [22] and adjusting them to the cement composition. Only potassium, sodium and hydroxyl ions were considered, as those are the major species usually found in the pore solution [22]. Table 3 presents the estimated initial pore solution composition.

During the experiments, once the power was switched on, ionic transport took place: lithium ions moved into and through the specimen, towards the cathode, while sodium and potassium ions moved mostly in the same direction. A part of these ions, however,

*Table 3: Estimated initial pore solution chemical composition*

| Ion           | Concentration (mol/l) |
|---------------|-----------------------|
| $\text{K}^+$  | 0.25                  |
| $\text{Na}^+$ | 0.20                  |
| $\text{OH}^-$ | 0.45                  |

leached to the anolyte. Hydroxyl ions moved towards the anode. At the electrodes, hydroxyl ions were either consumed (at the anode) or produced (at the cathode). In addition, a part of the lithium ions was most likely (chemically and/or physically) bound to the pore walls.

A 1-D multi-ion model was implemented using the Nernst-Planck mode in COMSOL Multiphysics® software. Three domains were considered: anolyte, specimen and catholyte. In the solution domains, Eq.(1) was applied for each species but the hydroxyl ions. In the specimen domain, on the other hand, Eq.(9) was used for each ion, except for the hydroxyl ions. In the case of the hydroxyl ions, both in bulk solutions and in pore solution, the transport equations were not used. The electroneutrality principle was considered to be valid and, thus, it was considered that there would be enough hydroxyl ions to balance out the positive charge of the cations (whose transports were calculated by the conservation equations). Therefore, the concentrations of hydroxyl ions were calculated from the electroneutrality equation (Eq.(2)). The use of the electroneutrality equation in order to calculate the concentration of one of the ions in the system, eliminating one of the conservation of mass equations, is known as the Equation Elimination Method (EEM) [26] and it is the default method in COMSOL's Nernst-Planck mode.

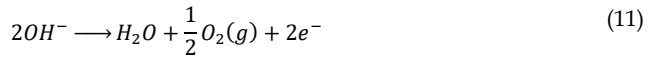
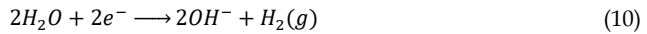
Transport by advection is not likely to happen under the present conditions [13]. Therefore, the advective term was considered to be zero in all domains. The specimen was considered to be fully saturated (saturation degree of one). The porosity of the specimen was estimated to be 20%.

Finally, the tortuosity-constrictivity factor was calculated by Eq.(8), using the average value of resistivity during the experiment ( $39 \Omega.m$ ). The average resistivity was used instead of the initial value in order to consider resistivity variations due to temperature increase observed during the experiments. The obtained tortuosity-constrictivity factor was 78, which agrees with values found in literature (e.g. [16, 27]).

In a 1-D model, every domain must have the same cross-sectional area, which is not the case in the actual experiment. In the specimen, ions transport only occurs in the pore solution, which represents only 20% of the actual specimen volume. If the volume of the modelled specimen domain was considered to be the whole actual specimen volume, concentrations would be five times smaller than if only the liquid volume was considered.

Using smaller concentrations for the sample domain would lead to errors in the interfaces cell-sample (especially when calculating the diffusion term, where concentration gradient has an important role). Alternatively, the length of the specimen domain could be decreased by five, keeping the concentrations as found in the pore solution. However, this approach would change the distance between the electrodes and would modify the shape of the profiles. Therefore, in order to take the different cross-sectional areas from pore solution and electrolyte chambers into account, the modelled anolyte and catholyte compartments were five times longer than their actual sizes (36 mm), with 180 mm each. Even though the modelled compartments were five times longer, their cross-sections were five times smaller, matching the cross-section of the liquid in the specimen. Thus, the volume of the cells remained unaltered. That way, the concentrations in the electrolyte domains and in the specimen were compatible. The specimen length was maintained the same (50.0 mm) and the electrodes (that is, points where voltage was applied) were placed at 2.0 mm from both ends of the specimen domain. Like in the experiments, the specimens were tested under 40 V for a week and the potential gradient between the electrodes was considered constant.

During a migration experiment, the following reactions take place at the cathode and anode, respectively:



that is, there is a hydroxyl sink in the anolyte and a hydroxyl source in the catholyte. The reaction rates of hydroxyl ions ( $R_{OH^-}$ , in mol/m<sup>3</sup>.s) in the electrolytes were calculated by:

$$R_{OH^-,anolyte} = -\frac{i_c}{d.F} \quad (12)$$

$$R_{OH^-,catholyte} = \frac{i_c}{d.F} \quad (13)$$

where  $d$  (in m) is the length of the region where the reaction took place. In this case, the adopted value was 1 mm.

The binding of lithium ions to the solid was also considered. When ions penetrate into concrete, they may interact chemically and/or physically with the cement matrix, leaving

the pore solution. This process depends not only on the nature of the species and its concentration, but also on factors such as temperature and concrete (mortar) composition [22]. However, there is no available information on lithium binding in the current literature. Therefore, in this paper, binding was assumed to be linearly proportional to lithium concentration in the pore solution. Thus, in the specimen domain, the reaction term was:

$$R_{Li^+, spec} = k_{lin}c_{Li^+} \quad (14)$$

where  $k_{lin}$  is a binding coefficient, in  $s^{-1}$ . In this work, three binding coefficients were evaluated: 0 (no binding),  $1.0 \times 10^{-7} s^{-1}$  and  $2.0 \times 10^{-7} s^{-1}$ . The chosen linear binding coefficients were such that the average final lithium contents in the specimen after migration were close to what was experimentally observed. The concentration of bound lithium,  $Li_b$ , in mol/kg of solid, was calculated by:

$$(1 - p)\rho \frac{\partial Li_b}{\partial t} = k_{lin}c_{Li^+} \quad (14)$$

where  $\rho$  is the density, in  $kg/m^3$ . In this work, mortar density was considered to be  $2160 kg/m^3$ .

## 5 Results and discussion

The results for the case with 4.9 M LiOH anolyte solution are initially presented. The current density plots obtained during the experiments and estimated by the model can be seen in Figure 2. The overall trend of the model results is similar to what was observed experimentally. In the model the specimen was considered to be fully saturated from the start, which led to the highest current as soon as the test began. In the experiment, however, as the specimens were not initially fully saturated, it took a couple of hours before the peak value could be reached. The same was experimentally observed by Pacheco and Polder [4]. Nevertheless, in both model and experiments, after the point of highest value, the current density slowly decreased and then became nearly constant. Interestingly, the current density values predicted by the model are close to the values observed during Experiment (II). The influence of lithium binding can be observed from day 5 on, with lower current densities as the binding coefficient increased.

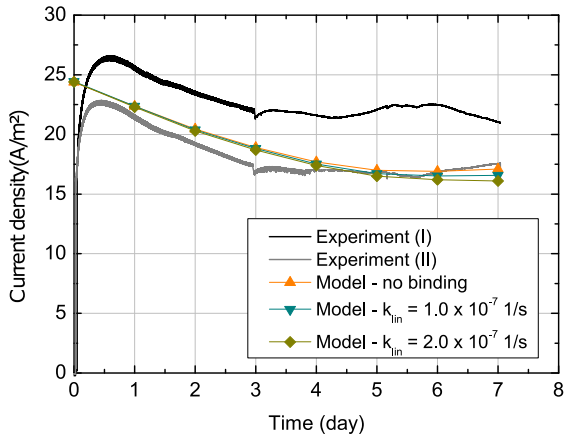


Figure 2: Current density passing through the specimen - comparison among model and experimental results

The estimated concentrations of sodium and potassium in the catholyte solutions obtained by the model also agree well with the results from the experiments, especially in Experiment (I) (Figure 3). Both model and experimental results show the accumulation of those ions in the catholyte over time. The model results are similar to what was experimentally observed, especially in Experiment (I). In this case, the sodium plots are close for the whole experiment while the potassium plots are close until day three. Nevertheless, the final model and experimental concentrations differ by less than 10%, in the case of Experiment (I). Interestingly, results show that sodium ions left the specimen at lower rate than potassium ions, probably due to lower concentration and mobility. Lithium binding had little influence on the sodium and potassium concentrations in the catholyte estimated by the model.

In contrast, the effect of lithium binding can clearly be observed in the concentrations of lithium in the catholyte (Figure 3). As expected, the higher is the binding coefficient, the less ions leave the specimen into the catholyte solution. This can be noted especially by the end of the experiment. Interestingly, for all model cases, it took six days for lithium ions to arrive in the catholyte. This behaviour is quite close to what was experimentally observed. However, all final concentrations (with or without binding) are much higher than the experimental ones. This could be related to the shape of the lithium profile in the specimen, as will be discussed further.

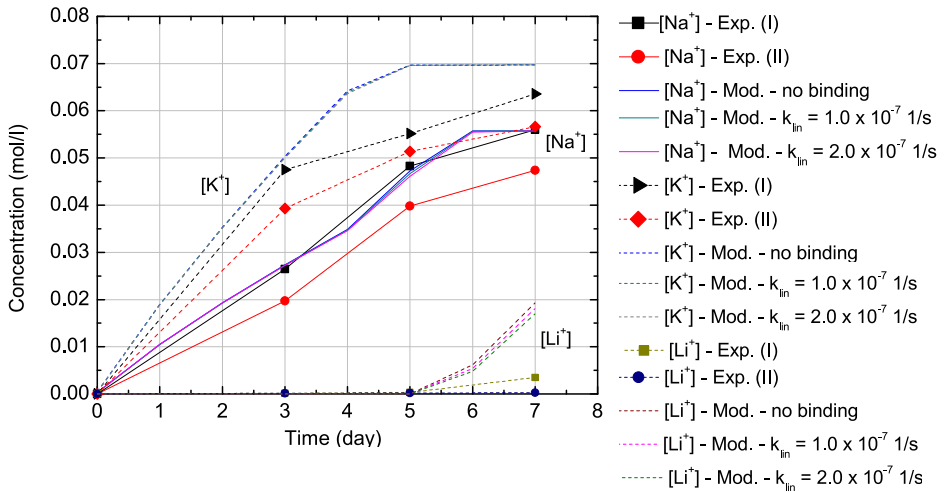


Figure 3: Sodium, potassium and lithium concentrations in the catholyte - comparison between experimental results and model calculations. The plots of the model results with different binding coefficients are overlapping for sodium and potassium.

Table 4 shows average total lithium (that is, the combination of ions in the pore solution and bound ions) content in the specimens after migration. The values estimated by the model agree well with the experimental values. Figure 4 shows the comparison between experimental and numerical total lithium profiles in the specimens. Overall, the profiles have similar shape, with a drop in concentration towards the cathode. However, the model underestimates the concentration in the region between 5 and 25 mm from the anode and overestimates it in the rest of the specimen. As the calculated concentration is overestimated in the region closer to the catholyte, it is likely that lithium concentrations in the catholyte are also higher than experimentally found, as seen in Figure 3.

Interestingly, other authors have used similar multi-ionic transport models to predict chloride migration in concrete and have obtained solutions with similar shape, regardless of considering binding (e.g. [16, 28]) or not (e.g. [17, 18]). Krabbenhøft and Krabbenhøft [17] attributed this shape to electroneutrality - the limited supply of cations would limit the transport of the anions, such as chlorides, in the system. Spiesz et al. [14], on the other hand, credit the differences between model and experimental profiles to wrong assumptions regarding binding and equilibrium between free and bound ions (chlorides, in the case of his work). Indeed, as previously mentioned, due to lack of investigations on lithium binding in the literature, considering it to be linearly proportional to the

concentration is a first approach. Therefore, further investigation is needed in order to obtain models that predict more realistic lithium concentration profiles.

Table 4: Average total lithium content in specimens after migration – comparison between experimental and model results

|   | Average total lithium (g/kg solid) |
|---|------------------------------------|
| No binding                                    | 0.34                               |
| $k_{lin} = 1.0 \times 10^{-7} \text{ s}^{-1}$ | 0.39                               |
| $k_{lin} = 2.0 \times 10^{-7} \text{ s}^{-1}$ | 0.48                               |
| Experimental (I)                              | 0.49                               |
| Experimental (II)                             | 0.31                               |

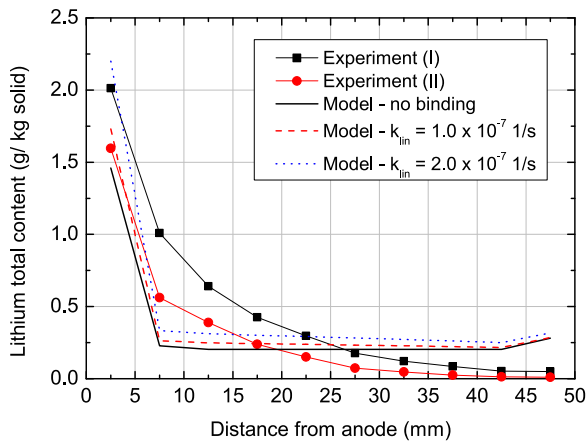


Figure 4: Final total lithium profiles in specimens – comparison between experimental and model results

Concentration profiles of sodium, potassium, lithium ions in the pore solution during migration, calculated by the model, are shown in the graphs of Figures 5, 6 and 7, respectively. As expected, sodium and potassium were attracted by the cathode and progressively left the specimen. All sodium left the pore solution before day six, while all potassium was depleted by day five. This agrees with the model predictions for the catholyte concentrations (see Figure 3) of those ions as their levels tend to stabilize by day six for sodium and by day five for potassium. As previously mentioned, potassium left the pore solution faster than sodium because of its higher mobility and concentration.

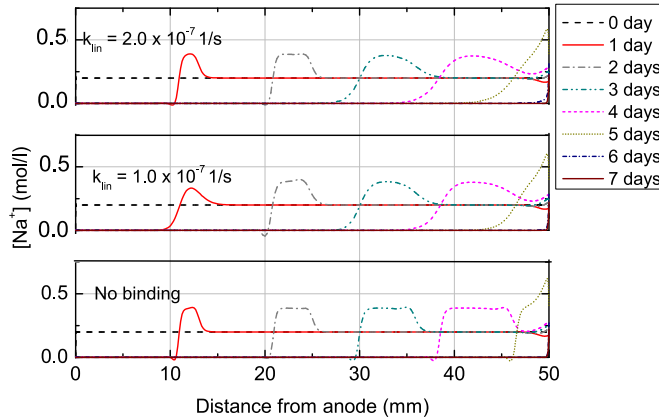


Figure 5: Model results for sodium concentration profiles in pore solution for three levels of lithium binding

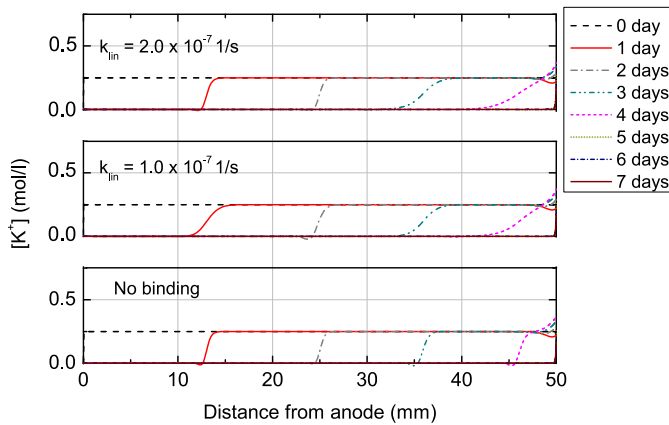


Figure 6: Model results for potassium concentration profiles in pore solution for three levels of lithium binding

As potassium moved faster towards the cathode, there was an area without potassium but with sodium. In that region, the sodium profile makes a hump, with higher concentration than initially. This probably happened due to the different mobilities of lithium, sodium and potassium. Lithium moves more slowly than sodium - therefore, there is an area where sodium is the only cation found. In that region, part of the current is carried by sodium ions and the rest, by hydroxyl ions. Therefore, there is an accumulation of sodium ions so that there are enough species to carry current in that area. Lithium binding had limited role on sodium and potassium profiles. With higher binding levels, the shape of the

profiles was slightly modified, especially from day three on. As lithium left the pore solution (due to being bound to the pore structure), in order to maintain electroneutrality, sodium and potassium had their transport slightly slowed down.

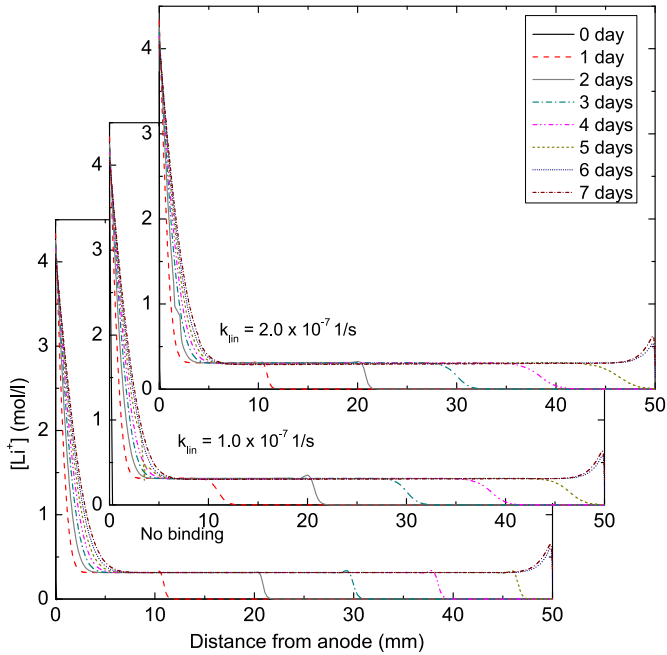


Figure 7: Model results for lithium concentration profiles in pore solution for three levels of lithium binding

Like in the total lithium profiles in Figure 4, the free lithium concentration profiles (Figure 7) have, initially, three different regions: a steep drop, followed by a region of constant lithium levels and finally the concentration decreases again. With time, the whole profile advances towards the cathode. In fact, the end of lithium profiles coincides with the beginning of areas with sodium. This is confirmed by the fact that lithium arrives in the catholyte before day six - the same time when all sodium has been removed from the pore solution. Therefore, according to the model, in order for lithium ions to advance in the specimen, it is necessary that sodium and potassium ions are first removed from its pore solution. This could limit or hinder the treatment, especially when the reinforcement is used as cathode. In this case, sodium and potassium are not removed from the pore solution - instead, they accumulate in the area around the cathode [29]. This should be considered when designing a possible treatment. Regarding lithium binding, as expected,

it modifies the lithium concentration profiles - the higher the binding coefficient, the lower levels of lithium were observed in the pore solution.

The hydroxyl concentration profiles in the specimens are shown in Figure 8. The profiles are combinations of the profiles from the positive ions (sodium, potassium and lithium), because hydroxyl concentrations were calculated using the electroneutrality principle (Eq. (2)). It is important noting that, even though hydroxyl has the highest mobility in the system, its transport (both in concentration and speed) was limited by the transport of the cations in the system. This is a direct consequence of a multi-ion model [17].

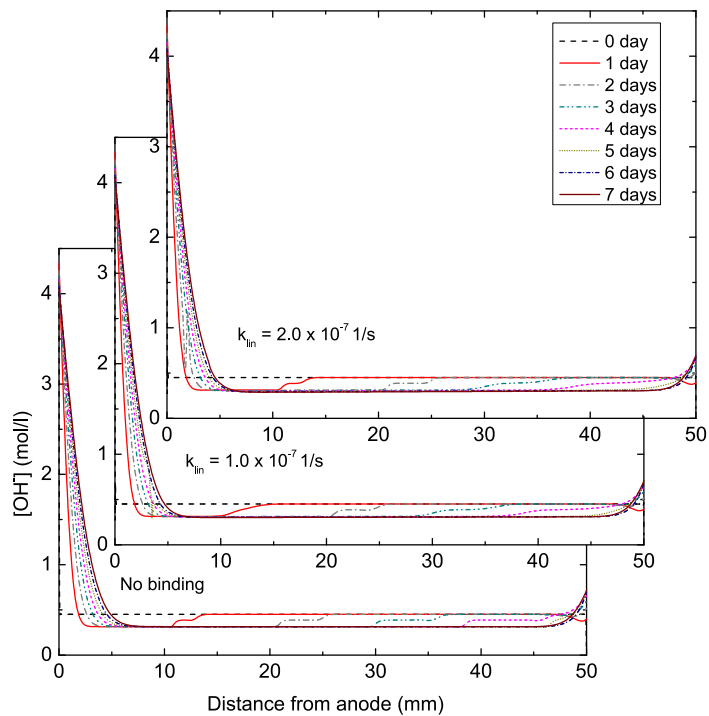


Figure 8: Model results for hydroxyl concentration profiles in pore solution for three levels of lithium binding

Figure 9 shows the modelled and experimental concentrations of lithium in the anolyte. In the model results, lithium concentrations decreased with time, as the ions left the anolyte and migrated into the specimen. Lithium binding did not affect much those concentrations - they practically coincide. When comparing to the experimental results, nevertheless, a clear difference can be noted. Indeed, the increase in lithium concentration experimentally

observed was not expected and it was likely due to water evaporation from the solution. The reduction of the anolyte volume led to the concentration increase. In contrast, in the model, the volume of the solution was considered constant.

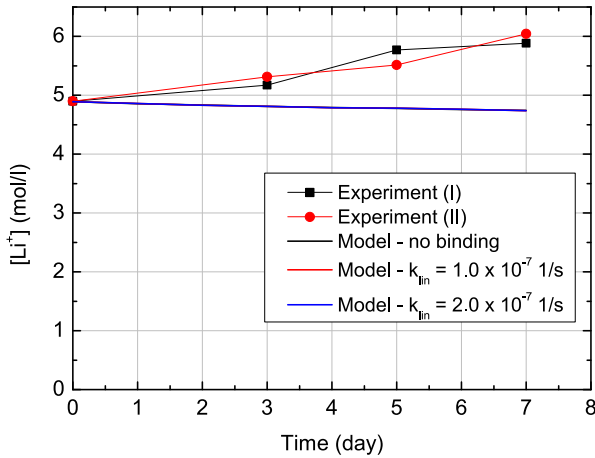


Figure 9: Lithium concentrations in anolyte - comparison between experimental results and model calculations. The plots of the model results with different binding coefficients are overlapping.

Sodium and potassium concentrations in the anolyte from the model are much lower than the ones observed during the experiments, as seen in Figure 10. The difference can be explained by the fact that highly concentrated alkali hydroxide solutions are known for attacking concrete, dissolving hydrated phases [30, 31]. As the anolyte was a very concentrated LiOH solution, it is possible that the attack took place during the experiment. In fact, during the experiments, calcium ions were also detected in the anolyte solutions, which also indicates that alkaline dissolution may have occurred. Nevertheless, the attack reaction was not considered in the model, leading to the underestimation of the concentration of sodium and potassium ions. In addition, it is interesting to note that, like in the case of anolyte lithium concentration, lithium binding had a limited role in the transport of those ions into the anolyte as the concentrations calculated by the model practically coincide.

The proposed model can also be used to estimate lithium migration during other experiments. The model (without binding) was used to estimate lithium transport during the experiment LiOH 0.2 M. As the discussion of these results is very similar to the previous case, a summary with the main model and experimental results is shown

in Table 5. It is interesting to notice that the behaviour of sodium and potassium ions described by the model is very close for both LiOH 0.2 M and 4.9 M cases, as it was

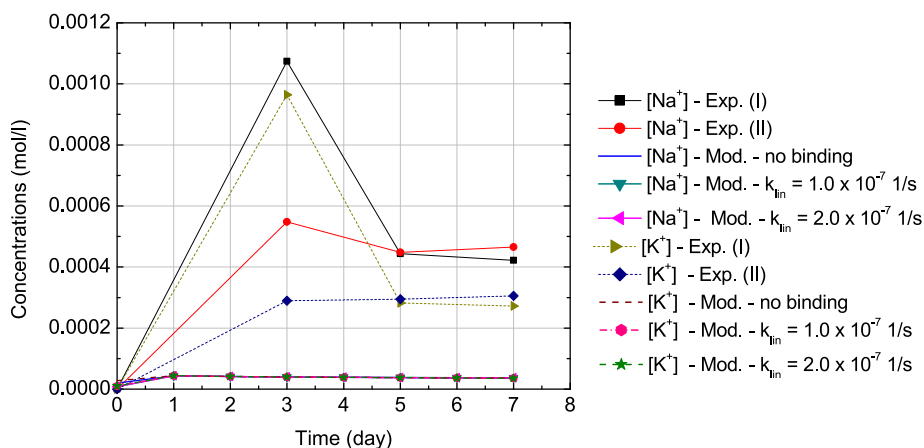


Figure 10: Sodium and potassium concentrations in the anolyte - comparison between experimental results and model calculations. The plots from the model results with different binding coefficients are overlapping.

Table 5: Summary of the main model and experimental results for the experiments with LiOH 0.2 M and LiOH 4.9 M as anolyte

|   | LiOH 0.2 M           |                      |                      |
|---|----------------------|----------------------|----------------------|
|   | Model                | Exp.                 |                      |
| Av. Li content in specimen (g/kg solid) | 0.19                 | 0.22                 |                      |
| Av. current density (A/m <sup>2</sup> ) | 17                   | 20                   |                      |
| Final catholyte [K] (mol/l)             | 0.07                 | 0.06                 |                      |
| Final catholyte [Na] (mol/l)            | 0.06                 | 0.05                 |                      |
| Final catholyte [Li] (mol/l)            | $7.2 \times 10^{-3}$ | $5.6 \times 10^{-3}$ |                      |
|   | LiOH 4.9 M           |                      |                      |
|   | Model                | Exp. (I)             | Exp. (II)            |
| Av. Li content in specimen (g/kg solid) | 0.34                 | 0.49                 | 0.31                 |
| Av. current density (A/m <sup>2</sup> ) | 19                   | 23                   | 19                   |
| Final catholyte [K] (mol/l)             | 0.07                 | 0.06                 | 0.06                 |
| Final catholyte [Na] (mol/l)            | 0.06                 | 0.06                 | 0.05                 |
| Final catholyte [Li] (mol/l)            | $1.9 \times 10^{-2}$ | $3.4 \times 10^{-3}$ | $2.9 \times 10^{-4}$ |

experimentally observed. This could indicate that the alkali removal does not greatly depend on the concentration of the anolyte solution. In general, the model estimated well the overall behaviour of ions during migration for both solutions. In the case of LiOH 4.9 M solution, even though experimental results presented limited variation between replicates, probably due to differences in the material (e.g. porosity), the model results presented in Table 5 fit in between them.

## 6 Conclusions

In this paper, a multi-ion numerical model for lithium transport under an electrical potential gradient was proposed. Lithium binding was assumed to be linearly proportional to lithium concentration at the studied rates as a first approach, due to lack of information on this topic in current literature. The model provided further understanding of mechanisms that occurred during lithium migration experiments and the following conclusions can be drawn.

- The model estimated well overall ionic transport during migration. Parameters such as current density, average total lithium content and sodium and potassium concentrations in the catholyte solutions obtained by the model were in good agreement to what was experimentally observed.
- Even though the model predicted well the average total amount of lithium in the specimen, it did not predicted very well how those ions are distributed throughout the specimen. This could be due to model assumptions, such as linear lithium binding or no binding at all. Further investigation is needed in order to obtain more realistic lithium concentration profiles.
- While sodium and potassium concentration variations in the catholyte were well predicted by the model, lithium concentrations were overestimated, probably due to the simplifying assumptions of the model, in which the interactions between lithium ions and the pore structure, i.e. binding, were not considered or were approximated by linear binding rate.

- The concentration profiles predicted by the model suggest that it is necessary that all sodium and potassium is removed from the pore solution before lithium ions can reach the catholyte.
- Differences between model and experimental results of the concentrations in the anolyte solutions highlighted mechanisms that possibly occurred during testing, namely water evaporation and alkali attack of the mortar, which were not considered in the model.
- The suggested model was be used to estimate lithium transport in other experiments. When calculating for the case when LiOH 0.2 M solution was used as anolyte, modelled and experimental results matched well. Lithium migration was greatly influenced by the lower concentration of the anolyte, while the transport of potassium and sodium was similar to the case with LiOH 4.9 M.

### *Acknowledgment*

This work was supported by Dutch Technology Foundation (STW), Sika Technology AG, BAM Infraconsult BV, Rijkswaterstaat, TNO Delft, Van Nieuwpoort Grint en Zand B.V. and TCKI - Stichting Technisch Centrum voor de Keramische Industrie (STW IS2C project 10971: "Modelling, non-destructive testing and Li-based remediation of deleterious Alkali-Silica Reaction in concrete structures").

## References

- [1] M. Thomas, D. Stokes, Lithium impregnation of ASR-affected concrete: preliminary studies, in: Proceedings of the 12th International Conference on Alkali-Aggregate Reaction in Concrete, 2004, pp. 659 – 667.
- [2] A. Santos Silva, M. Salta, M. Melo Jorge, M. Rodrigues, A. Cristino, Research on the suppression expansion due to ASR. Effect of coatings and lithium nitrate, in: Proceedings of the 13<sup>th</sup> International Conference on Alkali-Aggregate Reaction in Concrete, 2008.
- [3] D. Whitmore, S. Abbott, Use of an applied electric field to drive lithium ions into alkali-silica reactive structures, in: Proceedings, 11<sup>th</sup> International Conference on Alkali-Aggregate Reaction, 2000, pp. 1089-1098.
- [4] J. Pacheco, R. B. Polder, Preliminary study of electrochemical lithium migration into cementitious mortar, in: 2<sup>nd</sup> International Symposium on Service Life Design for Infrastructures, RILEM Publications SARL, 2010, pp. 1093-1100.
- [5] T. Ueda, J. Kushida, M. Tsukagoshi, A. Nanasawa, Influence of temperature on electrochemical remedial measures and complex deterioration due to chloride attack and ASR, *Construction and Building Materials* 67, 2014, pp. 81-87.
- [6] C.-C. Liu, W.-C. Wang, C. Lee, Behavior of cations in mortar under accelerated lithium migration technique controlled by a constant voltage, *Journal of Marine Science and Technology* 19 (1), 2011, pp. 26-34.
- [7] L. M. Souza, R. B. Polder, O. Çopuroğlu, Lithium migration in a two-chamber set-up as treatment against expansion due to alkali-silica reaction, *Construction and Building Materials* 134, 2017, pp. 324-335.
- [8] K. Ramyar, O. Çopuroğlu, Ö. Andiç, A. Fraaij, Comparison of alkali-silica reaction products of fly-ash- or lithium-salt-bearing mortar under long-term accelerated curing, *Cement and Concrete Research* 34 (7), 2004, pp. 1179-1183.
- [9] X. Feng, M. Thomas, T. Bremner, B. Balcom, K. Folliard, Studies on lithium salts to mitigate ASR-induced expansion in new concrete: a critical review, *Cement and Concrete Research* 35 (9), 2005, pp. 1789-1796.
- [10] X. Feng, M. Thomas, T. Bremner, K. J. Folliard, B. Fournier, New observations on the mechanism of lithium nitrate against alkali silica reaction (ASR), *Cement and Concrete Research* 40 (1), 2010, pp. 94-101.
- [11] K. J. Folliard, M. D. Thomas, B. Fournier, K. E. Kurtis, J. H. Ideker, Interim recommendations for the use of lithium to mitigate or prevent alkali-silica reaction (ASR), Tech. Rep. FHWA-HRT-06-073, Federal Highway Administration, 2006.

- [12] F. Rajabipour, E. Giannini, C. Dunant, J. H. Ideker, M. D. Thomas, Alkali-silica reaction: Current understanding of the reaction mechanisms and the knowledge gaps, *Cement and Concrete Research* 76, 2015, pp. 130-146.
- [13] C. Andrade, J. M. Diez, A. Alaman, C. Alonso, Mathematical modelling of electrochemical chloride extraction from concrete, *Cement and Concrete Research* 25 (4), 1995, pp. 727 - 740.
- [14] P. Spiesz, M. M. Ballari, H. Brouwers, RCM: a new model accounting for the non-linear chloride binding isotherm and the non-equilibrium conditions between the free-and bound chloride concentrations, *Construction and building materials* 27 (1), 2012, pp. 293-304.
- [15] B. Šavija, M. Luković, E. Schlangen, Lattice modeling of rapid chloride migration in concrete, *Cement and Concrete Research* 61, 2014, pp. 49-63.
- [16] M. Aguayo, P. Yang, K. Vance, G. Sant, N. Neithalath, Electrically driven chloride ion transport in blended binder concretes: Insights from experiments and numerical simulations, *Cement and Concrete Research* 66, 2014, pp. 1-10.
- [17] K. Krabbenhöft, J. Krabbenøft, Application of the Poisson-Nernst-Planck equations to the migration test, *Cement and Concrete Research* 38 (1), 2008, pp. 77-88.
- [18] E. Samson, J. Marchand, K. Snyder, Calculation of ionic diffusion coefficients on the basis of migration test results, *Materials and Structures* 36 (3), 2003, pp. 156-165.
- [19] L. M. Souza, R. B. Polder, O. Çopuroğlu, The influence of the anolyte solution type and concentration on lithium migration in mortar specimens, *Construction and Building Materials* 186, 2018, pp. 123-130.
- [20] J. Newman, K. E. Thomas-Alyea, *Electrochemical systems*, John Wiley & Sons, 2012.
- [21] W. J. Moore, *Physical chemistry*, Englewood Cliffs, New Jersey: Prentice-Hall, Inc., 1962.
- [22] L. Bertolini, B. Elsener, P. Pedferri, E. Redaelli, R. B. Polder, *Corrosion of steel in concrete: prevention, diagnosis, repair*, 2<sup>nd</sup> Edition, John Wiley & Sons, 2013.
- [23] J. M. Paz-Garcia, A. Riberio, J. M. Rodriguez-Maroto, B. Johannesson, L. M. Ottosen, Physicochemical and numerical modeling of electrokinetics in inhomogenous matrices, Ph.D. thesis, Technical University of Denmark, 2012.
- [24] ASTM-C1202-05, Standard test method for electrical indication of concrete's ability to resist chloride ion penetration, 2005.
- [25] N.-E. 196-1:2005, Methods of testing cement - part 1: Determination of strength, 2005.
- [26] F. Gagnon, D. Ziegler, M. Fafard, Electrochemical modelling using electroneutrality equation as a constraint, *Journal of Applied Electrochemistry* 44 (3), 2014, pp. 361-381.
- [27] S. Ahmad, A. K. Azad, K. F. Loughlin, Effect of the key mixture parameters on tortuosity and permeability of concrete, *Journal of Advanced Concrete Technology* 10 (3), 2012, pp.86-94.

- [28] O. Truc, J.-P. Ollivier, L.-O. Nilsson, Numerical simulation of multi-species transport through saturated concrete during a migration testMsDiff code, *Cement and Concrete Research* 30 (10), 2000, pp. 1581-1592.
- [29] L. M. Souza, R. B. Polder, O. Çopuroğlu, The effect of an embedded cathode on lithium migration in mortar specimens, *HERON* 62 (2), 2017, pp. 99-117.
- [30] H. F. Taylor, *Cement chemistry*, Thomas Telford, 1997.
- [31] P. Hewlett, *Lea's chemistry of cement and concrete*, Butterworth-Heinemann, 2003.